AGU FALL MEETING
Online Everywhere | 1–17 December 2020

DI011-0008

Magma Storage System and Hidden Hotspot Track of the Emeishan Large Igneous Province (ELIP) and its Impact on the Unusual Timing of the Capitanian Mass Extinction

Yiduo Liu (1), Lun Li (2), Jolante van Wijk (3), Aibing Li (1), Yuanyuan Fu (4)

(1) University of Houston; (2) Sun Yat-sen University; (3) New Mexico Institute of Mining and Technology; (4) China Earthquake Administration

Summary

Large igneous provinces (LIPs) are often associated with mass extinctions and are thus important for the evolution of life on Earth. However, the precise relation between LIPs and their impacts on biodiversity is enigmatic as they can be asynchronous. If environmental impacts are primarily related to sill emplacement, the structure of LIPs' magma storage system becomes critical as it dictates the occurrence and timing of mass extinction. Here we use surface wave tomography to image the lithosphere under the Permian Emeishan Large Igneous Province (ELIP) in SW China. We find a NE-trending zone of high shear-wave velocity (Vs) and negative radial anisotropy (Vsv > Vsh) in the lithosphere and interpret it as a mafic-ultramafic, dike-dominated magma storage system on the Emeishan hotspot track. An area of less-negative radial anisotropy, on the hotspot track but away from the major eruption center, reflects an elevated proportion of sills emplaced before or at the onset of the ELIP. Liberation of greenhouse gases and mercury by the sills explains why the mid-Capitanian global biota crisis preceded the major ELIP eruption by 2-3 million years.

1. Scientific questions and geological background

Questions:

- What is the form of the magma storage system of ELIP in the lithosphere?

- Why did the mass extinction event precede the peak time of ELIP?

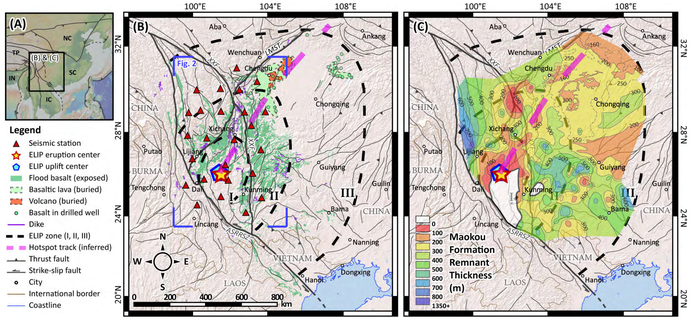

ELIP geological background:

- at least ~2.5-3 × 10^5 km^2 in the western Yangtze craton
- three concentric zones (inner, intermediate, outer), flood basalt thickness decreases outward
- most likely a mantle plume origin during northward drift of the South China block
- equatorial paleo-latitude at time of eruption, overall ~27-degree clockwise rotation since 260 Ma
- northeast-trending, anomalously thinned swath in the underlying Permian Maokou Formation
- northeast-trending, positive residual gravitational anomaly at the same place
- magmatic underplating, shown by high density, high velocity, high Vp/Vs ratios, thickened crust
- caused a global mass extinction event in the mid-Capitanian (ca. 262 Ma)
- peak activity (260-257 Ma) younger than the mass extinction

2. Shear wave velocity model of the lithosphere under ELIP

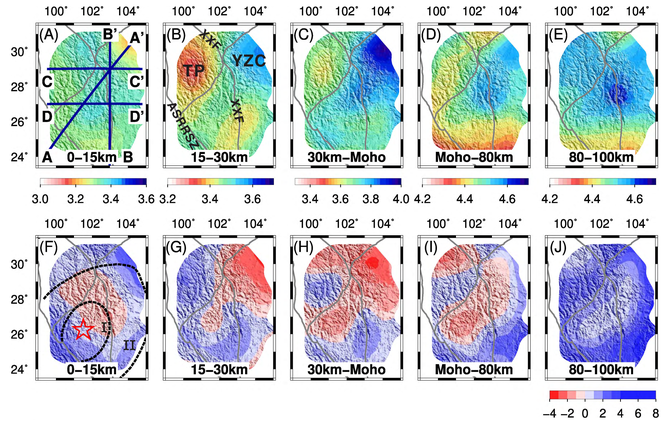

Observations (expected)

[1] high velocity at 15-220 km beneath the Yangtze craton east of XXF

[2] low velocity zone in the SE Tibetan crust

[3] Positive (Vsh > Vsv) radial anisotropy (100%*(Vsh-Vsv)/Vs) zones in the SE Tibetan crust and the western Yangtze crust

[4] Ubiquitous positive radial anisotropy in the lithospheric mantle below 80 km

Corresponding interpretations

[1] old, cold, and thick cratonic lithosphere

[2] overthickened, partially-molten middle to lower crust in SE Tibet

[3] sub-horizontal alignment of mica due to ductile deformation associated with the lateral expansion of Tibetan Plateau

[4] lattice preferred orientation of olivine in the horizontal plane

Observations (unexpected)

A NE-trending coherent zone of negative radial anisotropy (Vsv > Vsh) exists, associated with a high velocity anomaly. It shows as a broad zone in shallow crust (0-15 km) and can be traced downward to ~80 km depth. This zone of reduced radial anisotropy is still detectable down to 120 km depth within the Yangtze craton. The amplitude of the negative radial anisotropy is mostly -2% but is as strong as -4% in the lower crust under the Sichuan Basin.

Issues in geological interpretation

Crustal faults and cracks cannot explain the observed high velocity + negative radial anisotropy that extends into the Yangtze cratonic mantle lithosphere. Lithospheric-scale faulting, with possible partial melts from SE Tibetan Plateau, is also problematic because (1) the negative radial anisotropy body intersects with XXF and AASRRSZ at high angles, (2) lithospheric-scale, high-strain (say, >50%) structures within the craton that could generate the vertical alignment are not observed, and (3) such interpretations would produce low, rather than high, shear-wave velocities.

3. Tectonic interpretation and environment implications

(A) Effects of mafic-ultramafic intrusions on seismic properties (bulk shear-wave velocity and radial anisotropy)

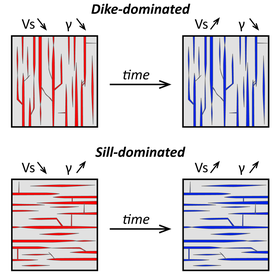

(B) Plate reconstruction at 260 Ma with velocity vectors. "North" in Permian is "Northeast" at present in South China due to overall clockwise rotation since then

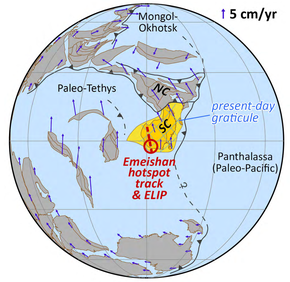

(C) Present-day section along the hidden hotspot track, characterized by dikes and sills in magma storage system of the ELIP

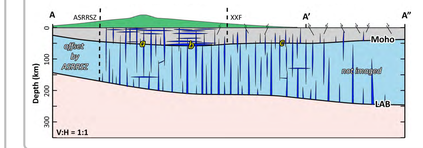

(D) Plume-lithosphere interaction processes

266(?) Ma: minor volcanism, rifting, uplifting, and karstification in Sichuan Basin; magma penetration is largely impeded by the thick lithosphere.

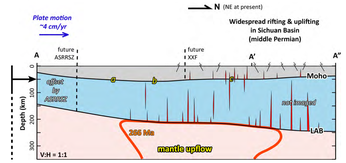

263 Ma: emplacement of dikes throughout the thinner lithosphere and sills in the upper crust and at the Moho ("b", underplating), associated with rifting and ore deposits; greenhouse gases and mercury are liberated, causing catastrophic environmental change and the mid-Capitanian mass extinction.

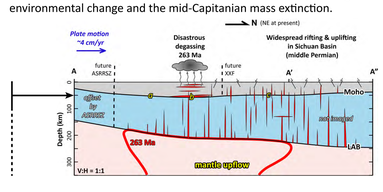

260 Ma: peak time of the ELIP activity at even thinner lithosphere, extensive flood basalt erupted; release of volatiles and mercury continued; this model explains the unusual temporal relationship between the mass extinction and the major ELIP eruption.

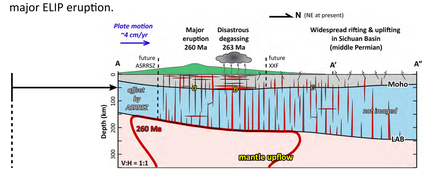

Key references

Bond, D. P., Wignall, P. B. & Grasby, S. E. The Capitanian (Guadalupian, Middle Permian) mass extinction in NW Pangea (Borup Fiord, Arctic Canada): A global crisis driven by volcanism and anoxia. Geol. Soc. Am. Bull. B35281.1 (2019).

Chung, S. L. & Jahn, B. M. Plume-lithosphere interaction in generation of the Emeishan flood basalts at the Permian-Triassic boundary. Geology 23(10), 889-892 (1995).

He, B., Xu, Y. G., Chung, S. L., Xiao, L. & Wang, Y. Sedimentary evidence for a rapid, kilometer-scale crustal doming prior to the eruption of the Emeishan flood basalts. Earth Planet. Sc. Lett. 213(3-4), 391-405 (2003).

Huang, H., Yao, H. & van der Hilst, R. D. Radial anisotropy in the crust of SE Tibet and SW China from ambient noise interferometry. Geophys. Res. Lett. 37(21), L21310 (2010).

Huang, B. et al. Paleomagnetic constraints on the paleogeography of the East Asian blocks during Late Paleozoic and Early Mesozoic times. Earth-Sci. Rev. 186, 8-36 (2018).

Shellnutt, J. G., Denyszyn, S. W. & Mundil, R. Precise age determination of mafic and felsic intrusive rocks from the Permian Emeishan large igneous province (SW China). Gondwana Res. 22(1), 118-126 (2012).

Wignall, P. B. et al. Volcanism, mass extinction, and carbon isotope fluctuations in the Middle Permian of China. Science 324(5931), 1179-1182 (2009).

Xie, J. et al. Crustal radial anisotropy across eastern Tibet and the western Yangtze craton. J. Geophys. Res-Solid Earth 118(8), 4226-4252 (2013).

Xu, Y. G., He, B., Chung, S. L., Menzies, M. A. & Frey, F. A. Geologic, geochemical, and geophysical consequences of plume involvement in the Emeishan flood-basalt province. Geology 32(10), 917-920 (2004).

Zhou, M. F. et al. A temporal link between the Emeishan large igneous province (SW China) and the end-Guadalupian mass extinction. Earth Planet. Sc. Lett. 196(3-4), 113-122 (2002).

Acknowledgments: Data used in the study were collected by the MIT-CIGMR seismic network and archived at the IRIS Data Management Center. Lun Li is funded by the NSFC (Grant No. 41804043, 41874102) and the Second Tibetan Plateau Scientific Expedition and Research Program (STEP) (Grant No. 2019QZKK0701). Yiduo Liu thanks the GURI Fund to Prof. John Suppe from the State of Texas and the University of Houston.

Appendix: method and tests

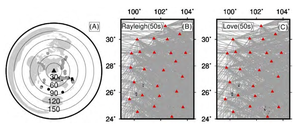

Distribution of tele-seismic events used for Rayleigh wave (black and gray solid circles) and Love wave tomography (gray solid circles only).

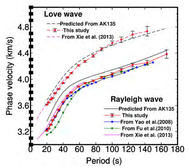

Average Rayleigh wave and Love wave phase velocities at 18 periods from 20 s to 143 s in the study region.

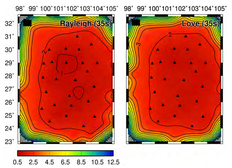

Distribution of 2 x standard error (σ) (%) of Rayleigh wave and Love wave phase velocity perturbation at 35 s.

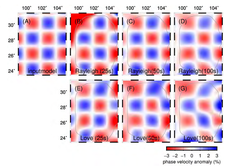

Input and recovered checkerboard models for resolution tests on Rayleigh wave and Love wave phase velocities.

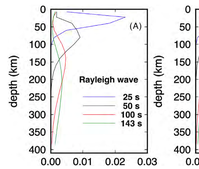

Sensitivity kernels of Rayleigh wave and Love wave with respect to isotropic (A) Vsv and (B) Vsh based on shear velocity model AK135 (Kennett et al., 1995).

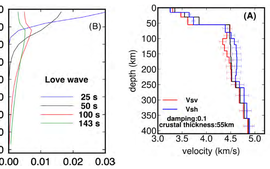

(A) 1-D averaged Vsv and Vsh profiles. Black solid line denotes AK135 model. Crustal thickness used for inversion is 55 km. (B) Observed (dots) and predicted (lines) average Rayleigh wave and Love wave phase velocities in the study region.

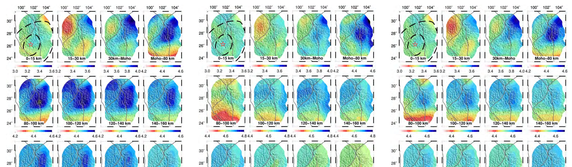

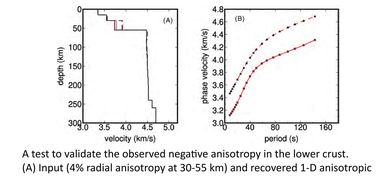

A test to validate the observed negative anisotropy in the lower crust. (A) Input (4% radial anisotropy at 30-55 km) and recovered 1-D anisotropic model. Black: input. Red: recovered. Solid & dashed lines: Vsh & Vsv. (B) Rayleigh wave (square) and Love wave (triangle) phase velocities calculated from the input anisotropic model. Red solid and dashed curves are predictions from the recovered model from the joint inversion.